



# Flow-pattern-altered syntheses of core–shell and hole–shell microparticles in an axisymmetric microfluidic device

Duo Wang<sup>1,2,4</sup> · Xu Zheng<sup>2</sup> · Xiaodong Chen<sup>3</sup> · Guoqing Hu<sup>1</sup>

Received: 21 February 2021 / Revised: 27 March 2021 / Accepted: 14 April 2021 / Published online: 1 July 2021  
© The Chinese Society of Theoretical and Applied Mechanics and Springer-Verlag GmbH Germany, part of Springer Nature 2021

## Abstract

Droplet-based microfluidics offers unique advantages to create platforms that fabricate functionalized particles with increased accessibility, robustness, and simplicity. Herein we present a three-phase microfluidic device that can control the flow pattern to directly generate either core–shell or hole–shell microparticles. The major benefits of this device are the ease of controlling the morphology of the compound droplets by the flow rates and thus the microstructure of the synthesized microparticles. The transition between flow patterns enables the generation of either core–shell particles or Janus particles in a single device. We further show the versatility of the proposed device in fabrication of functionalized particles: the hole size of the hole–shell microparticle can be fine-tuned while its outer diameter is kept constant, and by adding Fe<sub>3</sub>O<sub>4</sub> nanoparticles into the photocurable phase, the obtained magneto-responsive microparticle can move rotationally or translationally under an external magnetic field. We anticipate that the present method could facilitate the fabrication of the functional microparticles for diverse applications.

**Keywords** Microfluidics · Droplet · Microparticle · Janus particle

## 1 Introduction

Microparticles with tunable sizes, structures [1–4], and functions have important applications in the fields of drug delivery [5–9], controlled release [10–14], drug identification [15], biological diagnosis [3, 16], stabilizing liquid film [17], electrophoretic display [1, 18–20], and chemical

microreaction [21]. In term of controlling drug release, functional behaviors of microparticles are strongly influenced by their sizes and structures. For instance, the drug release rate is proportional to the size of microparticles [22–25], a core–shell structure can protect the active substances in the core against undesired degradation [26], a hole–shell structure can control the release of the core contents through the hole [27], and a Janus structure can provide two compartments for encapsulating two different active materials and release them simultaneously [28]. Various conventional methods, such as inkjet printing [29], spray drying [30, 31], interfacial polymerization [32], membrane emulsification [33], were used to produce microparticles.

Recently, droplet-based microfluidics emerges as a powerful platform for generating highly monodisperse emulsion droplets in a controllable way [34–38]. Microdroplets are perfect templates for producing uniformly sized microparticles with different morphologies and functions. The size of synthesized microparticles can be precisely controlled by adjusting the flow rates [39, 40]. By photocuring the ultraviolet (UV)-curable phase of the core–shell droplets generated in axisymmetric capillary microfluidic devices, core–shell microparticles [26, 39, 41] can be synthesized. By changing the adhesion energy between the inner droplet

---

Executive Editor: Hong-Yuan Jiang

✉ Xiaodong Chen  
xiaodong.chen@bit.edu.cn

✉ Guoqing Hu  
ghu@zju.edu.cn

<sup>1</sup> State Key Laboratory of Fluid Power and Mechatronic Systems, Department of Engineering Mechanics, Zhejiang University, Hangzhou 310027, China

<sup>2</sup> State Key Laboratory of Nonlinear Mechanics (LNM), Institute of Mechanics, Chinese Academy of Sciences, Beijing 100190, China

<sup>3</sup> School of Aerospace Engineering, Beijing Institute of Technology, Beijing 100081, China

<sup>4</sup> School of Engineering Science, University of Chinese Academy of Sciences, Beijing 100049, China

and the outer phase, core–shell droplets can gradually evolve into Janus droplets for synthesizing hole–shell microparticles [42]. However, different fractions of ethoxylated trimethylolpropane triacrylate (ETPTA) monomer in the oil phase are needed to generate hole–shell microparticles with different shapes. Hole–shell microparticles can also be generated by gas–liquid Janus emulsions [9] or by solvent evaporation from core–shell microdroplets [43]. Still, these methods require the use of a gas or an easily vaporized substance as the inner phase, which brings in extra technical complication.

Microparticles can be functionalized for specific applications during synthesis [44]. Decorating chemical functional groups or molecules on the surface of microparticles can give them desired properties [45]. For instance, photo- and thermoresponsive microparticles synthesized by photochromic ploy (*N*-isopropylacrylamide-*co*-spironaphthoxazine methacryloyl) (PNIPA-SPO) copolymer will change their color when exposed to UV–Vis irradiation, and change their volume and color when exposed to temperature change [46]. Microparticles modified with MnO<sub>2</sub> nanoparticles on the surface can be used as micromotors, which push themselves forward through bubbles generated by the decomposition of hydrogen peroxide catalyzed by MnO<sub>2</sub>, for wastewater treatment [47]. By adding quantum dots and Fe<sub>3</sub>O<sub>4</sub> nanoparticles to distinct hemispherical compartments respectively, the Janus microparticles can realize fluorescent display under a magnetic field [48]. Magnetic micro-grippers synthesized by temperature-responsive hydrogel materials and Fe<sub>3</sub>O<sub>4</sub> nanoparticles can achieve drug capture and loading and targeted release under the synergistic control of temperature and magnetic field [9].

Herein, we demonstrate a flow-pattern-altered synthesis of core–shell and hole–shell microparticles in a single axisymmetric microfluidic device, which is different from the existing works that can only synthesize one type of microparticle in the same device. Benefiting from the precise control of fluids in microfluidic capillaries, the morphology of the compound droplets can be easily tailored by tuning the flow rates. Compared with the existing methods, the present approach can continuously produce microparticles with desired structures in a relatively simple way. The resultant core–shell microparticles with adjustable hole size or magneto-responsive microparticles doped with Fe<sub>3</sub>O<sub>4</sub> nanoparticles could be ideal microcarriers for drug delivery.

## 2 Experimental section

### 2.1 Microfluidic device fabrication

The fabrication of the capillary microfluidic device follows the standard procedure [39, 49]. The borosilicate circular

capillaries with an outer diameter of 0.96 mm and an inner diameter of 0.55 mm were pulled by a micropipette puller (P-97, Sutter Instrument Co., USA) to form capillaries with a tapered tip. The tips were scored and broken into a size of 20–200 μm with a clean 90° break technique [50] using a ceramic tile (Agilent Technologies, Inc., USA). Tips larger than 200 μm, which usually do not have a 90° break, require polishing on a sandpaper to form smooth cross-section at the final tips. The capillary microfluidic devices were fabricated by aligning two circular capillaries with different tip sizes inside a square tube with inner height of 1 mm. The circular capillary with a smaller tip size was used as the injection capillary, while another circular capillary with a larger tip size was used as the collection tube. Since the inner height of the square capillary is slightly larger than the outer diameters of the circular capillaries, it is easy to align the two circular capillaries in the square capillary. Note that the wetting condition of the capillaries plays an important role in stable and controllable generation of compound microdroplets. After being soaked in ethanol for 1 h, rinsed with deionized water, soaked again in 20% NaOH solution for 5 h, and rinsed thoroughly with deionized water, all the surfaces of the capillaries were assured to be hydrophilic. The assembling was accomplished at the stage of an inverted microscope (Nikon Eclipse Ti, Nikon Instruments, Inc., Japan). The capillaries were positioned on the glass slide using an epoxy glue (5-min Epoxy®, Devcon, Illinois Tool Works, Inc., USA). The openings of the injection capillary and the square tube were covered by syringe needles. These needles were connected to the syringe pumps (Pump 11 Elite, Harvard Apparatus, Inc., USA) through the polypropylene tubes.

### 2.2 Reagents

Inspired by the work of Nisisako and Hatsuzawa [51], three types of reagents were used in the present experiments—silicone oil (Sigma-Aldrich, density 0.93 g/cm<sup>3</sup>, kinematic viscosity 10 cSt, USA) as the inner phase, a photocurable solution, a monomer, 1,6-hexanediol diacrylate (HDDA, density 1.02 g/cm<sup>3</sup>, dynamic viscosity 6.27 mPa s, Ryoji, Korea), with 1.0 wt% photoinitiator 2-hydroxyl-2-methylpropiophenone (Darocur 1173, Nanjing SciChe New Materials Technology Co., Ltd., Nanjing, China) as the middle phase, and the deionized water dissolved with 1.0 wt% sodium dodecyl sulfate (SDS, Shanghai Ekear Biotechnology Co., Ltd., Shanghai, China) and 60% glycerol (Sinopharm Chemical Reagent Co., Ltd., Shanghai, China) as the outer aqueous phase. The interfacial tensions between any two phases were measured at room temperature by a tensiometer (Attension theta, Biolin Scientific Ltd., Finland). The interfacial tension  $\sigma_{sw}$  at the silicone oil/water interface is 13.15 mN/m, the interfacial tension  $\sigma_{sm}$  at the silicone oil/monomer interface

is 1.89 mN/m, and the interfacial tension  $\sigma_{mw}$  at the monomer/water interface is 5.53 mN/m.

### 2.3 Generation of compound droplets and microparticles

The compound droplets were generated by delivering the three immiscible reagents through the microfluidic device using syringe pumps. As schematically illustrated in Fig. 1a, the circular capillary on the left (colored in blue) is used as the injection tube for silicone oil (inner phase, colored in yellow–orange and with volumetric flow rate of  $Q_1$ ). The circular capillary on the right (colored in yellow) is used as a collection tube to collect generated droplets. HDDA (middle phase, colored in red–purple and with volumetric flow rate of  $Q_2$ ) flows from left to right inside the gap between the outer surface of the injection capillary and the inner surface of the square tube. Aqueous phase (outer phase, colored in blue–green and with volumetric flow rate of  $Q_3$ ) flows from right to left inside the gap between the outer surface of the collection tube and the inner surface of the square capillary. These three phases meet at the junction between the tips of the injection and collection tubes to form a flow-focusing configuration. The generation of compound microdroplets was recorded using a high-speed charge coupled device (CCD) camera (Phantom V7.3, Vision Research, Inc., USA) and the Phantom Camera Control software (PCC 2.14, Vision Research, Inc., USA). The microdroplets were continuously photopolymerized in situ inside the collection tube by an UV light source (LC8, Hamamatsu Photonics, Shizuoka, Japan) to form microparticles. The microparticles were then collected and washed using ethanol to remove the non-curable reagents. The morphologies of the dried microparticles were examined with a scanning electron

microscope (Quanta 250 FEG, FEI Company, USA). As shown in Fig. 1b, we found that the flow pattern can be changed to a way in which the two dispersed phases align parallelly at the channel junction to generate Janus microdroplets, which allows the generation of microdroplets with two totally different morphologies in a single device.

## 3 Results and discussion

### 3.1 Morphologies of compound microdroplets

The formation of the compound microdroplets is due to the instability of the fluid interfaces. Pinched or sheared by the continuous phase through the orifice of the collection tube, the dispersed phases break into microdroplets. Based on the breakup position, the formation process of the microdroplets can be classified as dripping and jetting modes. In the dripping mode, the small perturbations on the interfaces cause microdroplets to be pinched off at a fixed spatial position near the orifice of the collection tube. In the jetting mode, the perturbations are amplified along the interfaces of the jet, forming less uniform microdroplets. The transition between these two modes is strongly affected by the velocities of the three phases. Adjusting their flow rates results in three types of compound microdroplets, i.e., multiple-core, core–shell, and Janus morphologies as depicted in Fig. 2a. Compound microdroplets with multiple-core and core–shell structure, have been widely observed in the previous works [49, 52–54]. Their formation depends on the relationship between the breakup frequencies of the inner and middle phases [54]. When the breakup frequency of the inner phase is higher than that of the middle one, one droplet of the middle phase encapsulates several droplets of the inner phase, generating multiple-core droplets. Note that the multiple-core droplet is caused by the jetting model that is not used for particle fabrication here. Differently, the inner and middle phases break simultaneously or sequentially to form core–shell droplets. Compound microdroplets with Janus structure is due to the change in flow pattern and will be discussed in the next section. Figure 2b shows a regime diagram of three morphologies for a fixed  $Q_3$ . In a wide range of  $Q_1$  (0.5–1.4 mL/h), the morphology of the compound droplets changes from Janus to core–shell and then to multiple-core as  $Q_2$  increases. When  $Q_1$  exceeds a critical value, the multiple-core morphology disappears as  $Q_2$  increases. Movies S1–S3 in the Supporting Information show the dynamic evolution of the three types of compound microdroplets.

The diameter of the compound droplet is determined by the flow rates of the three immiscible phases and the sizes of the capillary tips. We can readily adjust the flow rates

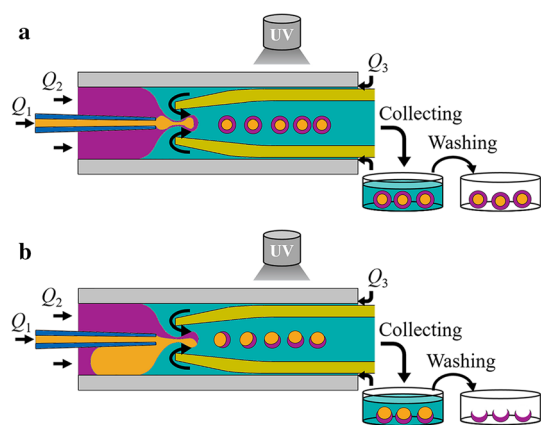


**Fig. 1** Schematic illustration of the generation of **a** core–shell and **b** Janus microparticles in a single microfluidic capillary device.  $Q_1$ ,  $Q_2$  and  $Q_3$  are the volumetric flow rates of the inner, middle, and outer phases, respectively

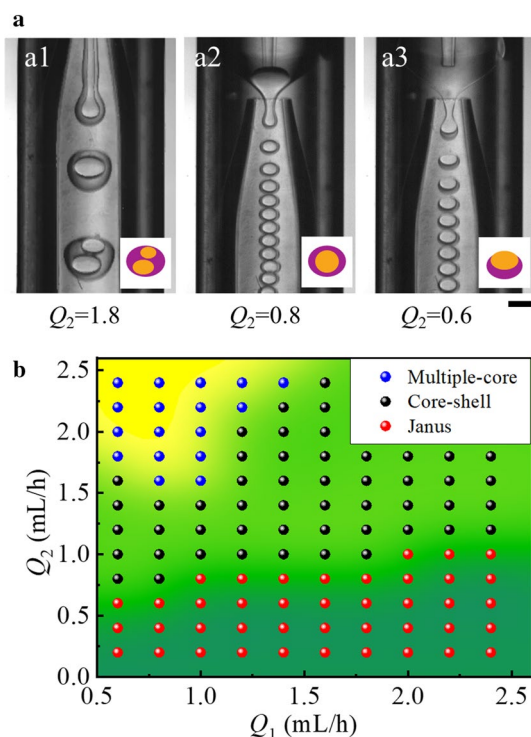


**Fig. 2** Generation of microdroplets with different morphologies. The outer and inner diameters of the tip of the collection tube are 425  $\mu\text{m}$  and 250  $\mu\text{m}$  respectively. **a** Three different generation patterns of compound droplets under different middle volumetric flow rate ( $Q_2$ ), with the same inner volumetric flow rate,  $Q_1=0.6$  mL/h and outer phase volumetric flow rate,  $Q_3=6$  mL/h. Subfigures **a1**, **a2**, **a3** correspond to multiple-core, core-shell, and Janus droplets, respectively. The scale bar is 200  $\mu\text{m}$ . See videos for the dynamic process of the generation of the three different compound droplets in Supporting Information (Movies S1–S3). **b** Regime diagram for droplet types as a function of  $Q_1$  and  $Q_2$ , where  $Q_3$  is fixed at 6 mL/h

or use a collection tube with a different tip to get larger or smaller compound droplets. Figure 3 displays the generation of the droplets with three morphologies in a device that has a smaller collection tip. Although the flow rate of the continuous phase is smaller than that used in Fig. 2, it can still generate smaller microdroplets. Without changing the flow rates of the inner phase and the continuous phase, the size of the compound droplets gradually decreases as the flow rate of the middle phase decreases (Fig. 3a). In fact, the size of the compound droplets also decreases if the flow rates of the inner phase or the continuous phase increase. A regime diagram of the morphologies of the compound microdroplets for a fixed  $Q_3$  can be obtained by gradually adjusting the flow rates of the inner and middle phases (Fig. 3b). The trend of the morphology evolution of the compound microdroplets is similar to that in Fig. 2b, demonstrating the robustness of the present microfluidic system.

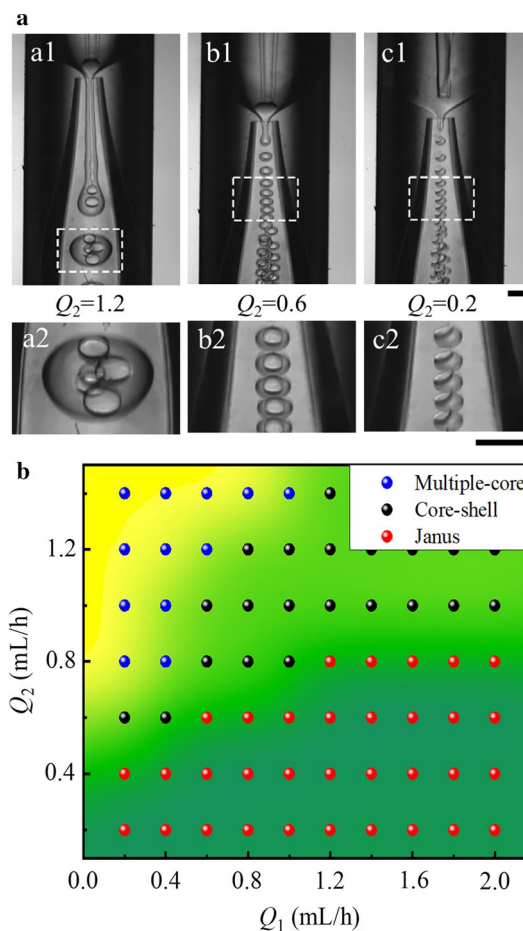


**Fig. 3** Generation of microdroplets with different morphologies in a device that has a smaller tip of the collection tube. The outer and inner diameters of the tip of the collection tube are 275  $\mu\text{m}$  and 170  $\mu\text{m}$ , respectively. **a** Three different generation patterns of compound droplets under different middle volumetric flow rate ( $Q_2$ ), with the same inner volumetric flow rate,  $Q_1=0.4$  mL/h and outer phase volumetric flow rate,  $Q_3=3$  mL/h. Subfigures **a2**, **b2**, **c2** correspond to for multiple-core, core-shell, and Janus droplets, respectively. Both scale bars are 200  $\mu\text{m}$ . **b** Regime diagram for droplet types as a function of  $Q_1$  and  $Q_2$ , where  $Q_3$  is fixed at 3 mL/h

### 3.2 Evolution of Janus mode

Direct generation of both core-shell and Janus microdroplets in the same microfluidic device, to the best of our knowledge, was observed in the present experiment for the first time. Besides, the transition of the compound droplet morphologies between core-shell and hole-shell can be realized by solely changing the flow pattern at the channel junction. Figure 4a shows again that, once the Janus microdroplet is generated, a large droplet of the inner phase always sticks at the upstream of the tip of the injection tube. This large droplet inclines to partially contact the outer wall of the injection tube and the inner wall of the square tube, therefore, the two dispersed phases form a side-by-side arrangement to create



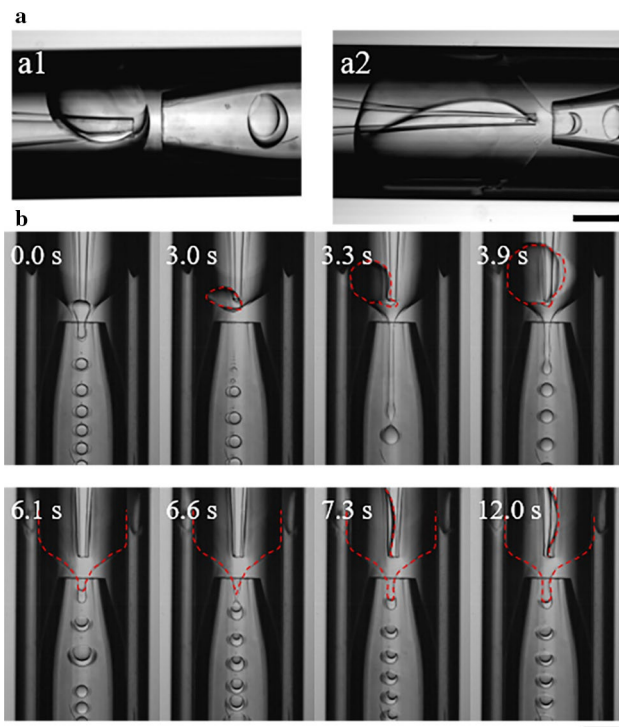


**Fig. 4** **a** Large droplet of inner phase located stably at the upstream of the channel junctions with two different sizes in the Janus mode. **b** Series of still images showing a formation process of the large droplet of the inner phase. The dashed red line highlights the interfaces observed from the side view. The scale bars are 400  $\mu\text{m}$

a triple-line at the junction of the three phases. The resulting compound droplets display the double-faced morphology, which is called the Janus mode.

To elucidate the occurrence of the Janus mode, we varied the flow rate of the inner phase to monitor how the core-shell mode transits to the Janus mode, as shown in Fig. 4b. The combination of the three flow rates is selected to be near the diagram boundary between the core-shell and Janus modes as provided in Fig. 2b. The dashed red line highlights the interfaces observed from the side view. The device initially generates core-shell droplets at  $t=0$  s. The flow rate of the inner phase then increases a bit to trigger the transition from the core-shell mode to the Janus one. At  $t=3.0$  s, the inner phase accumulates at the small orifice of the injection capillary, and the interface between the inner phase and the middle phase deforms rapidly under the action of the interfacial tension between the inner phase and middle phase. By contrast, the interface between the middle phase and the continuous phase deforms slowly because the square tube channel is much larger than the injection capillary orifice. The two interfaces approach each other but cannot directly touch each other. Since the interfacial tension between the inner phase and the middle phase is weaker than the interfacial tension between the middle phase

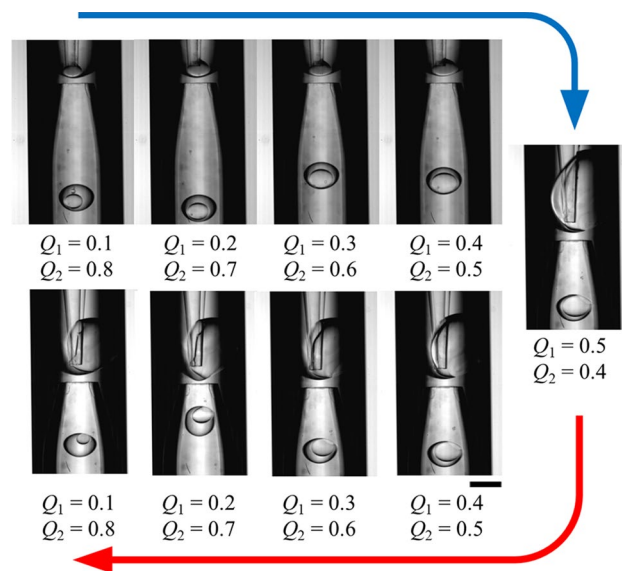


**Fig. 5** Generation of droplets with different morphologies at the same combination of the three flow rates. The total flow rate of  $Q_1$  and  $Q_2$  is maintained at 0.9 mL/h, and the continuous flow rate is fixed at 8 mL/h. Morphology of droplets evolves along the blue and red path. The scale bar is 550  $\mu\text{m}$

and the continuous phase, the pressure of the inner phase cannot push the interface between the middle phase and the continuous phase to move downward. Therefore, the interface between the inner phase and the middle phase can only deforms backward. At  $t=3.3$  s and 3.9 s, the droplet of inner fluid continues to grow and finally occupies the cross-section of the square tube. The middle phase is solely stretched by the outer phase to form a momentary jetting mode. At  $t=6.1$  s, the droplet of inner fluid becomes large enough to move downwards and is stretched by the flow field. The interface between the innermost and middle phases contacts the interface between the middle and continuous phases to form a three-phase contact line. A side-by-side distribution of the inner and middle fluids thus generates compound droplets with side-by-side morphology, i.e., Janus droplets. Close observation shows that the inner and middle phases break in an alternate way. The shapes of the large droplet and the generated Janus droplets become steady at  $t=12$  s, suggesting the complete transition of the core-shell mode to the Janus mode.

### 3.3 Generation of core-shell and Janus droplets at the same flow rates

Thanks to the adhesive force experienced by the large droplet at the channel wall in the Janus mode, we can even produce compound droplets with different morphologies under the same combination of flow rates. Figure 5 shows the generation process of the compound droplets in dripping mode,

under  $Q_1 + Q_2 = 0.9$  mL/h and  $Q_3 = 8$  mL/h. Initially, the two interfaces do not contact with each other and the droplet of the inner phase is encapsulated inside the droplet of the middle phase. Therefore, the device generates core–shell microdroplets when  $Q_1 = 0.1$  mL/h ( $Q_2 = 0.8$  mL/h) at the beginning. As shown in the blue path, the core–shell microdroplets are generated until  $Q_1 = 0.5$  mL/h ( $Q_2 = 0.4$  mL/h), when the large droplet of the inner phase appears between the tip of the injection capillary and the inner wall of the square tube to change the flow pattern to the Janus mode. The inner phase is now connected with the inner wall of the square tube. As long as the large droplet of the inner phase keeps sticking on the capillary wall, compound microdroplets with different morphologies can be generated by decreasing  $Q_1$ . With further decreasing of  $Q_1$  along the red path shown in Fig. 5, the large droplet does not disappear but its size decreases. All the droplets shown in Fig. 5 can be stably generated for a long time (at least 1 h). Note that, if the large droplet of the inner phase is flushed away by a sudden increase of  $Q_2$ , the Janus mode will return to the core–shell mode again. In addition, the size of the compound microdroplets generated at such fixed combination of flow rates keeps almost the same, no matter how the ratio  $Q_1/Q_2$  changes. The thickness of the shell can be precisely controlled by varying  $Q_1/Q_2$ . Consequently, if the total flow rate of the two dispersed phases and the flow rate of the continuous phase are fixed, we can obtain the compound microdroplets with uniform size and different morphology.

### 3.4 Fabrication of core–shell and hole–shell microparticles

Microparticles were fabricated by photopolymerizing the UV-curable phase in the compound droplets in situ inside the collection tube by UV irradiation, as shown schematically in Fig. 1. Briefly, the UV light causes the initiator molecules to homolytic cleavage forming benzoyl radicals, which then react with monomer molecules by taking a  $\pi$  electron from the C=C bond at the end of the monomer molecule to form a C–C bond [41]. The remaining unpaired  $\pi$  electron on the C atom of the monomer molecules makes the entire monomer molecule into another radical. The size and morphology of the resulting microparticles are controlled by the compound microdroplets, i.e., core–shell droplets for core–shell particles and Janus droplets for hole–shell particles. It should be noted that the hole–shell microparticles were fabricated by in situ curing the compound microdroplets that have not yet been able to evolve to the final equilibrium morphology, which is determined by the minimization of the interfacial free energies. The collected microparticles were washed with the absolute ethanol for several times to clean off the silicone oil and glycerin–water solution remaining on the particle surface (schematically shown in Fig. 6). Figure 6a

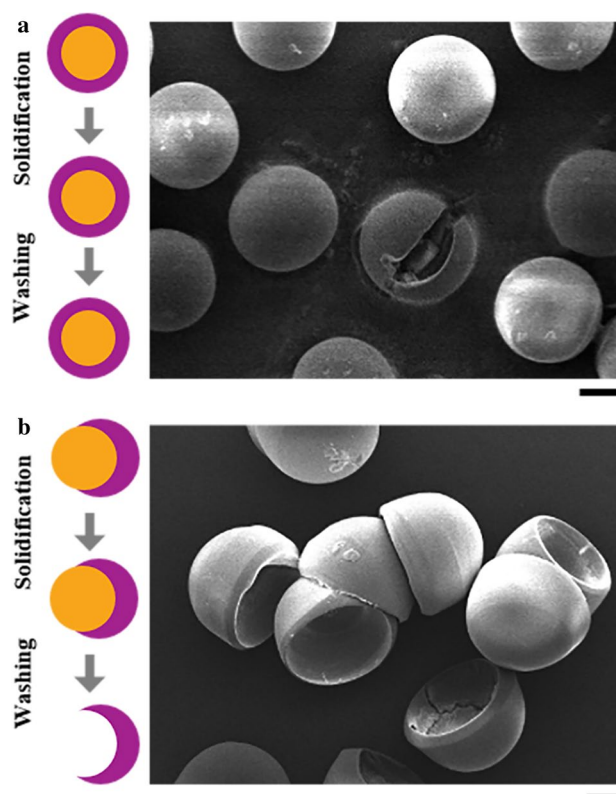


**Fig. 6** Scanning electron microscope (SEM) images of the microparticles. **a** Core–shell microparticles synthesized from core–shell microdroplets. **b** Hole–shell microparticles synthesized from Janus microdroplets. The scale bars are 150  $\mu$ m

shows the scanning electron microscope (SEM) image of the core–shell microparticles, one of which was stabbed to show the encapsulation of the silicone oil and the core–shell morphology. Figure 6b shows the SEM image of hole–shell microparticles fabricated from Janus microdroplets. These SEM images confirm that the sizes and shapes of the synthesized microparticles are highly uniform.

### 3.5 Controlling the hole size of microparticle

Janus microdroplets are spherical immediately after their formation since the balancing of the three interfaces at the triple-line cannot reach the steady state yet. Cured by UV light in situ, the generated hole–shell microparticles then have nearly spherical shape. The holes in the shell can facilitate mass transport through the shell for selectively capturing particles for classification and separation [42], confined synthesis of functional materials [42], and controlled release of molecules and nanoparticles [27]. The size of the hole also plays an important role in controlling the kinetics of drug release [25]. Here we further explored the possibility to tune the hole size. As demonstrated in the previous part, we can always change the shell thickness of the droplets

while keep the size of droplets at the same time. Figure 7a, b shows the Janus droplets and the corresponding synthesized hole-shell microparticles generated under the same  $Q_3$ , as well as the same sum of  $Q_1$  and  $Q_2$ . When the ratio of  $Q_1/Q_2$  is changed from 1:2 to 2:1, the hole size becomes larger. We measured the holes and diameters of these microparticles and found that the sizes of hole differ significantly (145  $\mu\text{m}$

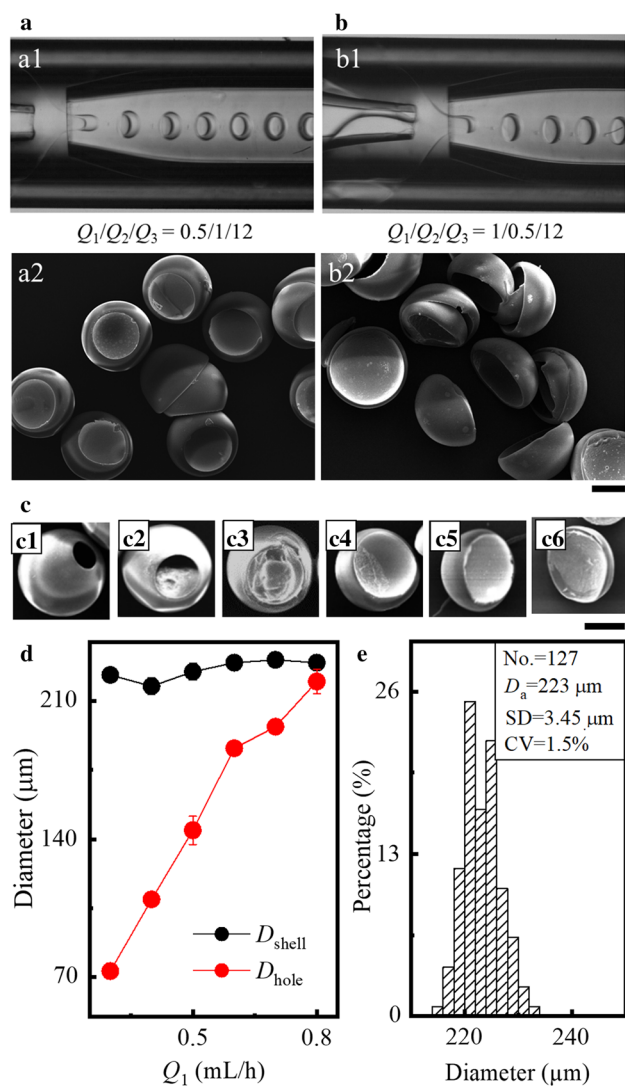


**Fig. 7** Controlling the hole size of microparticles. **a, b** Generations of hole-shell microparticles under  $Q_1 + Q_2 = 1.5$  mL/h and  $Q_3 = 12$  mL/h, but different  $Q_1$  and  $Q_2$ . **a1** and **b1** are experimental snapshots and **a2** and **b2** are SEM images corresponding to **a1** and **b1**. **c** Series of SEM images showing that shapes of microparticles change from hole-shell to shallow-bowl-like as the  $Q_1$  increases under  $Q_1 + Q_2 = 1$  mL/h and  $Q_3 = 9$  mL/h. **d** Variations of shell diameters and hole diameters corresponding to **c**. **e** Distribution of the shell diameters for the microparticles generated under  $Q_1 = 0.3$  mL/h,  $Q_2 = 0.7$  mL/h and  $Q_3 = 9$  mL/h. The average diameter ( $D_a$ ) of 127 shells is 223  $\mu\text{m}$ , with a standard deviation (SD) of 3.45  $\mu\text{m}$ . The coefficient of variation (CV) of the shell diameters is 1.5%. The scale bars are 100  $\mu\text{m}$

vs. 200  $\mu\text{m}$ ) while the diameters of particles are very close (210  $\mu\text{m}$  vs. 225  $\mu\text{m}$ ).

We prepared a series of microparticles under  $Q_1 + Q_2 = 1$  mL/h and  $Q_3 = 9$  mL/h. Figure 7c shows that the opening of microparticles increases with  $Q_1$  and the morphology of the microparticles gradually change from hole-shell to crescent-moon shape. The measurements in Fig. 7d confirm that the hole size increases monotonically while the shell diameter keeps about  $225 \pm 7$   $\mu\text{m}$ . To show the monodispersity of the generated microparticles, Fig. 7e gives the distribution of the shell diameters of the microparticles generated under  $Q_1 = 0.3$  mL/h and  $Q_2 = 0.7$  mL/h. The small coefficient of variation (CV) of 1.5% confirms that the present capillary microfluidic device can produce highly monodisperse microparticles.

### 3.6 Magnetic response of hole-shell microparticles

By adding magnetic  $\text{Fe}_3\text{O}_4$  nanoparticles into the monomer solution, we synthesized magnetoresponsive hole-shell microparticles from Janus droplets. Figure 8 shows the orientations of two types of hole-shell microparticles without and with the external magnetic field in the ethanol solution, respectively. Figure 8a1 shows that, in the absence of a magnetic field, the holes of the hole-shell microparticles generated under  $Q_1/Q_2 = 1$  face upward in the solution because of the uneven distribution of the magnetic nanoparticles in the asymmetrical structure. Here

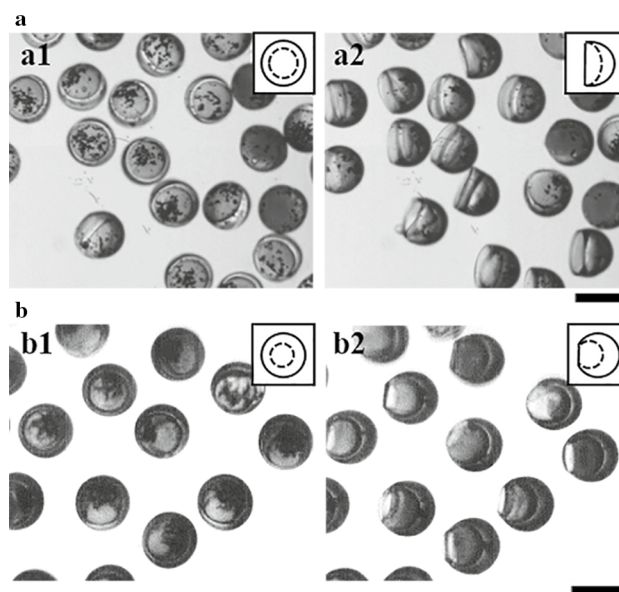


**Fig. 8** Orientation of the hole-shell microparticles without and with an external magnetic field. **a** Holes face upward without a magnetic field (**a1**) and rotate to the opposite direction of the magnetic field (**a2**). **b** Orientation of the smaller holes is similar to that of the bigger ones. Hole-shell microparticles were generated at  $Q_1/Q_2 = 1$ . The scale bars are 200  $\mu\text{m}$



the hole of the microparticle acts as the head of a roly-poly toy. When subjected to a magnetic field, the holes of the microparticles rotate to the opposite direction of the magnetic field, as shown in Fig. 8a2. After removing the external magnetic field, these roly-poly toys put themselves right again. For microparticles with smaller holes in Fig. 8b, we also observed a swift response of hole–shell microparticles to the external magnetic field. An animation of the hole–shell particles rotating under a rotating magnetic field is provided in the Supporting Information (Movie S4). These microparticles can be loaded with drug molecules or small drug particles after being immersed in an aqueous solution of drug and treated by ultrasonic vibration [27, 42]. Guided by a magnetic field, the magnetoresponsive motion of these microparticle could be used for targeted drug delivery.

## 4 Conclusions

This work describes an axisymmetric flow-focusing capillary microfluidic device that can produce either core–shell microparticles or hole–shell ones by only tuning the flow rates. The versatility of the device allowed the easy adjustment of the morphologies of the compound droplets and thus the structures of the resultant microparticles. We characterized the physical mechanism triggering the transition from the core–shell model to the Janus model. Different from the well-studied core–shell microdroplets, Janus microdroplets were formed with the presence of a large droplet of the inner phase near the entrance of the collecting capillary, causing two dispersed phases to align parallelly at the entrance. The hole–shell microparticles with nearly constant shell diameter but varied hole sizes were readily generated by adjusting the flow rates. In addition, the introduction of magnetic nanoparticles endowed the resultant microparticles with ability to move rotationally or translationally under external magnetic fields. This robust method that only controls the flow rates in a single microfluidic device could facilitate the fabrication of microparticles as ideal microcarriers for controlled drug delivery.

**Supplementary Information** The online version of this article (<https://doi.org/10.1007/s10409-021-01096-w>) contains supplementary material, which is available to authorized users.

**Acknowledgments** This work was supported by the National Natural Science Foundation of China (Grants 11832017, 11772343, and 12072350), the Chinese Academy of Sciences Key Research Program of Frontier Sciences (Grant QYZDB-SSW-JSC036), the Chinese Academy of Sciences Strategic Priority Research Program (Grant XDB22040403), and the Beijing Institute of Technology Research Fund Program for Young Scholars.

## References

- Han, S.W., Choi, S.E., Chang, D.H., et al.: Colloidal pixel-based micropatterning using uniform Janus microparticles with tunable anisotropic particle geometry. *Adv. Funct. Mater.* **29**, 1805392 (2019)
- Kamperman, T., Van Loo, B., Gurian, M., et al.: On-the-fly exchangeable microfluidic nozzles for facile production of various monodisperse micromaterials. *Lab Chip* **19**, 1977–1984 (2019)
- Lewis, C.L., Choi, C.H., Lin, Y., et al.: Fabrication of uniform DNA-conjugated hydrogel microparticles via replica molding for facile nucleic acid hybridization assays. *Anal. Chem.* **82**, 5851–5858 (2010)
- Hayakawa, M., Onoe, H., Nagai, K.H., et al.: Complex-shaped three-dimensional multi-compartmental microparticles generated by diffusional and Marangoni microflows in centrifugally discharged droplets. *Sci. Rep.* **6**, 1–9 (2016)
- Anselmo, A.C., Xu, X., Buerkli, S., et al.: A heat-stable microparticle platform for oral micronutrient delivery. *Sci. Transl. Med.* **11**, eaaw3680 (2019)
- Zhang, S., Zhou, S., Liu, H., et al.: Pinecone-inspired nano-architected smart microcages enable nano/microparticle drug delivery. *Adv. Funct. Mater.* **30**, 2002434 (2020)
- Liu, D., Zhang, H., Fontana, F., et al.: Microfluidic-assisted fabrication of carriers for controlled drug delivery. *Lab Chip* **17**, 1856–1883 (2017)
- Liu, X., Yang, H., Liu, Y., et al.: Numerical study of clathrin-mediated endocytosis of nanoparticles by cells under tension. *Acta Mech. Sin.* **35**, 691–701 (2019)
- Geng, Y.H., Ge, X.H., Zhang, S.B., et al.: Microfluidic preparation of flexible micro-grippers with precise delivery function. *Lab Chip* **18**, 1838–1843 (2018)
- He, F., Zhang, M.J., Wang, W., et al.: Designable polymeric microparticles from droplet microfluidics for controlled drug release. *Adv. Mater. Technol.* **4**, 1800687 (2019)
- Herranz-Blanco, B., Arriaga, L.R., Makila, E., et al.: Microfluidic assembly of multistage porous silicon-lipid vesicles for controlled drug release. *Lab Chip* **14**, 1083–1086 (2014)
- Amstad, E., Kim, S.H., Weitz, D.A.: Photo- and thermoresponsive polymersomes for triggered release. *Angew. Chem. Int. Ed.* **51**, 12499–12503 (2012)
- Yin, W.S., Yates, M.Z.: Encapsulation and sustained release from biodegradable microcapsules made by emulsification/freeze drying and spray/freeze drying. *J. Colloid Interface Sci.* **336**, 155–161 (2009)
- Cheng, P., Wang, X., Feng, C.: Numerical simulation of phosphorus release from resuspended sediment. *Acta Mech. Sin.* **36**, 1191–1201 (2020)
- Lyu, J., Ruan, C., Zhang, X., et al.: Microparticle-assisted precipitation screening method for robust drug target identification. *Anal. Chem.* **92**, 13912–13921 (2020)
- Miyata, T., Jige, M., Nakaminami, T., et al.: Tumor marker-responsive behavior of gels prepared by biomolecular imprinting. *Proc. Natl Acad. Sci. USA* **103**, 1190–1193 (2006)
- Wu, S., Yang, Y., Jiang, H.: Thinning air–water films stabilized by bacterial particles. *Acta Mech. Sin.* (2021). <https://doi.org/10.1007/s10409-020-01031-5>
- Song, J.K., Choi, H.J., Chin, I.: Preparation and properties of electrophoretic microcapsules for electronic paper. *J. Microencapsul.* **24**, 11–19 (2007)
- Nisisako, T., Torii, T., Takahashi, T., et al.: Synthesis of monodisperse bicolored Janus particles with electrical anisotropy using a microfluidic co-flow system. *Adv. Mater.* **18**, 1152–1156 (2006)



20. Nisisako, T.: Recent advances in microfluidic production of Janus droplets and particles. *Curr. Opin. Colloid Interface* **25**, 1–12 (2016)
21. Lan, Y., Yang, L., Zhang, M.C., et al.: Microreactor of Pd nanoparticles immobilized hollow microspheres for catalytic hydrodechlorination of chlorophenols in water. *ACS Appl. Mater. Interfaces* **2**, 127–133 (2010)
22. Berklund, C., Kim, K.K., Pack, D.W.: Fabrication of PLG microspheres with precisely controlled and monodisperse size distributions. *J. Control. Release* **73**, 59–74 (2001)
23. Berklund, C., King, M., Cox, A., et al.: Precise control of PLG microsphere size provides enhanced control of drug release rate. *J. Control. Release* **82**, 137–147 (2002)
24. Chen, W.L., Palazzo, A., Hennink, W.E., et al.: Effect of particle size on drug loading and release kinetics of gefitinib-loaded PLGA microspheres. *Mol. Pharm.* **14**, 459–467 (2017)
25. Qiu, J., Huo, D., Xue, J., et al.: Encapsulation of a phase-change material in nanocapsules with a well-defined hole in the wall for the controlled release of drugs. *Angew. Chem. Int. Ed.* **58**, 10606–10611 (2019)
26. Windbergs, M., Zhao, Y., Heyman, J., et al.: Biodegradable core-shell carriers for simultaneous encapsulation of synergistic actives. *J. Am. Chem. Soc.* **135**, 7933–7937 (2013)
27. Hyun, D.C., Lu, P., Choi, S.I., et al.: Microscale polymer bottles corked with a phase-change material for temperature-controlled release. *Angew. Chem. Int. Ed.* **125**, 10662–10665 (2013)
28. Kong, T., Liu, Z., Song, Y., et al.: Engineering polymeric composite particles by emulsion-templating: thermodynamics versus kinetics. *Soft Matter* **9**, 9780–9784 (2013)
29. Iwanaga, S., Saito, N., Sanae, H., et al.: Facile fabrication of uniform size-controlled microparticles and potentiality for tandem drug delivery system of micro/nanoparticles. *Colloids Surf. B* **109**, 301–306 (2013)
30. Hwang, Y.K., Jeong, U., Cho, E.C.: Production of uniform-sized polymer core-shell microcapsules by coaxial electrospinning. *Langmuir* **24**, 2446–2451 (2008)
31. Zhang, L., Huang, J., Si, T., et al.: Coaxial electrospay of microparticles and nanoparticles for biomedical applications. *Expert Rev. Med. Devices* **9**, 595–612 (2012)
32. Shenoy, R., Tibbitt, M.W., Anseth, K.S., et al.: Formation of core-shell particles by interfacial radical polymerization initiated by a glucose oxidase-mediated redox system. *Chem. Mater.* **25**, 761–767 (2013)
33. Dragosavac, M.M., Vladisavljević, G.T., Holdich, R.G., et al.: Production of porous silica microparticles by membrane emulsification. *Langmuir* **28**, 134–143 (2012)
34. Wu, H., Ren, Y.K., Hou, L.K., et al.: Fabrication of syntactic foam fillers via manipulation of on-chip quasi concentric nanoparticle-shelled droplet templates. *Lab Chip* **20**, 4600–4610 (2020)
35. Huang, F., Zhu, Z., Niu, Y., et al.: Coaxial oblique interface shearing: tunable generation and sorting of double emulsions for spatial gradient drug release. *Lab Chip* **20**, 1249–1258 (2020)
36. Mu, K., Ding, H., Si, T.: Experimental and numerical investigations on interface coupling of coaxial liquid jets in co-flow focusing. *Phys. Fluids* **32**, 042103 (2020)
37. Jiang, T., Jia, Y., Sun, H., et al.: Dielectrophoresis response of water-in-oil-in-water double emulsion droplets with singular or dual cores. *Micromachines* **11**, 1121 (2020)
38. Pang, Y., Wang, X., Liu, Z.: Study of droplet flow in a T-shape microchannel with bottom wall fluctuation. *Acta Mech. Sin.* **34**, 632–643 (2018)
39. Chen, P.W., Erb, R.M., Studart, A.R.: Designer polymer-based microcapsules made using microfluidics. *Langmuir* **28**, 144–152 (2012)
40. Kim, J.W., Utada, A.S., Fernandez-Nieves, A., et al.: Fabrication of monodisperse gel shells and functional microgels in microfluidic devices. *Angew. Chem. Int. Ed.* **119**, 1851–18554 (2007)
41. Al Nuumani, R., Bolognesi, G., Vladisavljević, G.T.: Microfluidic production of poly(1,6-hexanediol diacrylate)-based polymer microspheres and bifunctional microcapsules with embedded TiO<sub>2</sub> nanoparticles. *Langmuir* **34**, 11822–11831 (2018)
42. Wang, W., Zhang, M.J., Xie, R., et al.: Hole-shell microparticles from controllably evolved double emulsions. *Angew. Chem. Int. Ed.* **52**, 8084–8087 (2013)
43. Ekanem, E.E., Zhang, Z.L., Vladisavljevic, G.T.: Facile microfluidic production of composite polymer core-shell microcapsules and crescent-shaped microparticles. *J. Colloid Interface Sci.* **498**, 387–394 (2017)
44. Kim, D.Y., Jin, S.H., Jeong, S.G., et al.: Microfluidic preparation of monodisperse polymeric microspheres coated with silica nanoparticles. *Sci. Rep.* **8**, 1–11 (2018)
45. Jo, Y.K., Lee, D.: Biopolymer microparticles prepared by microfluidics for biomedical applications. *Small* **16**, 1903736 (2020)
46. Lone, S., Kim, S.H., Nam, S.W., et al.: Microfluidic preparation of dual stimuli-responsive microparticles and light-directed clustering. *Langmuir* **26**, 17975–17980 (2010)
47. Ren, M., Guo, W., Guo, H., et al.: Microfluidic fabrication of bubble-propelled micromotors for wastewater treatment. *ACS Appl. Mater. Interfaces* **11**, 22761–22767 (2019)
48. Yin, S.N., Wang, C.F., Yu, Z.Y., et al.: Versatile bifunctional magnetic-fluorescent responsive Janus supraballs towards the flexible bead display. *Adv. Mater.* **23**, 2915–2919 (2011)
49. Kim, S.-H., Kim, J.W., Kim, D.-H., et al.: Enhanced-throughput production of polymersomes using a parallelized capillary microfluidic device. *Microfluid. Nanofluid.* **14**, 509–514 (2013)
50. Oesterle, A.: *Pipette Cookbook 2018: P-97 & P-1000 Micropipette Pullers*. Sutter Instrument, Novato (2015)
51. Nisisako, T., Hatsuzawa, T.: A microfluidic cross-flowing emulsion generator for producing biphasic droplets and anisotropically shaped polymer particles. *Microfluid. Nanofluid.* **9**, 427–437 (2009)
52. Chu, L.Y., Utada, A.S., Shah, R.K., et al.: Controllable monodisperse multiple emulsions. *Angew. Chem. Int. Ed.* **119**, 9128–9132 (2007)
53. Nabavi, S.A., Vladisavljević, G.T., Gu, S., et al.: Double emulsion production in glass capillary microfluidic device: parametric investigation of droplet generation behaviour. *Chem. Eng. Sci.* **130**, 183–196 (2015)
54. Utada, A.S., Lorenceau, E., Link, D.R., et al.: Monodisperse double emulsions generated from a microcapillary device. *Science* **308**, 537–541 (2005)